Molecular Vision 2019; 25:194-203 <http://www.molvis.org/molvis/v25/194>
Received 22 August 2018 | Accepted 16 March 2019 | Published 18 March 2019

Reliability and reproducibility of a rodent model of choroidal neovascularization based on the subretinal injection of polyethylene glycol

Ivan Fernandez-Bueno,[1,2,3] Maria-Luz Alonso-Alonso,[1] Maria-Teresa Garcia-Gutierrez,[1] Yolanda Diebold[1,4]

[1]Instituto Universitario de Oftalmobiología Aplicada (IOBA), University of Valladolid, Valladolid, Spain; [2]Centro en Red de Medicina Regenerativa y Terapia Celular de Castilla y León, Valladolid, Spain; [3]Red Temática de Investigación Cooperativa en Salud (RETICS), OftaRed, Instituto de Salud Carlos III, Valladolid, Spain; [4]Biomedical Research Networking Center on Bioengineering, Biomaterials and Nanomedicine (CIBER-BBN), Valladolid, Spain

Purpose: To evaluate the reliability and reproducibility of a rodent choroidal neovascularization (CNV) model by subretinal injection of polyethylene glycol (PEG).

Methods: C57BL/6 mice were injected subretinally with 2 µl PBS (Gibco, Invitrogen, Paisley, UK; n=14) or PEG (1 mg; n=18). Animals were sacrificed at either 0, 5, 14 or 21 days. Eyes were embedded in paraffin wax and serial sections were stained with haematoxylin and eosin or Fontana-Masson or immunostained for cytokeratin 8/18, isolectin B4 (IB4), vascular endothelial growth factor (VEGF) and von Willebrand factor (vWF).

Results: Both the PBS and PEG groups had retinal degeneration and retinal pigment epithelium (RPE)/choroid modifications at 5 and 14 days. Pigment clumps and cell vacuolization at the RPE/choroid were identified as melanin-containing RPE cells. In PEG-injected eyes, CK8/18-positive cellular elements were present at the subretinal space, IB4 immunoreactivity was significantly increased and choroidal vessels appeared diffusely thickened. However, neither VEGF nor vWF (angiogenesis/neovascularization markers) were detected in either group. At 21 days, the retina/choroid of PBS-injected animals was normal in appearance, while retina/choroid changes remained in some PEG-injected mice.

Conclusions: Subretinal injection of PEG induced retina/choroid degenerative modifications that mimic the initial steps of human CNV. However, ocular changes were heterogeneous among animals from PBS and PEG groups and did not follow a consistent pattern while most PBS-injected animals showed similar degenerative changes. Abnormal growth of new vessels originating from the choroidal vasculature was not observed. Therefore, we consider that this model does not consistently reproduce CNV and that researchers should choose other rodent models of CNV to avoid misinterpreting their results.

Retinal and choroidal neovascularization can occur in association with numerous retinal diseases, such as retinopathy of prematurity, proliferative diabetic retinopathy and age-related macular degeneration (AMD), affecting people of all ages [1]. In parallel with increased human longevity, AMD will cause more vision loss than the combined effects of diabetes and glaucoma [2-5]. In 10%–15% of AMD cases, neovascularization, the inappropriate growth of new blood vessels, occurs [6,7]. Choroidal neovascularization (CNV), the principal form of neovascular AMD, is a chief cause of vision loss worldwide [8]. In CNV, abnormal new choroidal vessels invade the RPE, subretinal space or both [6]. In addition to this new vessel growth, anomalous extracellular deposits occur in the space between the RPE and Bruch's membrane [9-12]. The presence of the accumulated matter suggests a role in the development of CNV, but it is not known if it represents the cause of the disease, the effect or both [9-12]. Despite progress in preventing vision loss from AMD, especially by incorporating anti-vascular endothelial growth factor (VEGF) agents in clinical management stratagems, many patients will still have significant vision impairment [13]. Therefore, a need remains to better understand the pathogenesis of CNV that will also facilitate the identification of new therapeutic targets.

Animal models can provide valuable cellular and molecular insights regarding the pathogenesis of CNV. Such validated models can then be used to develop and test novel treatments. Some approaches to developing suitable animal models utilize internal interventions, such as genetic manipulations [14-17]. While undoubtedly useful, the manifestations

Correspondence to: Ivan Fernandez-Bueno; Instituto Universitario de Oftalmobiología Aplicada (IOBA), Paseo de Belén 14, University of Valladolid, Valladolid, 47011, Spain; Phone: +34 983184756 FAX: +34 983184762; email: ifernandezb@ioba.med.uva.es

of CNV in these models occur in only a small percentage of the animals, take a relatively long time to develop, and encompass a relatively small area of the retina [13].

In contrast to internal interventions, most CNV models rely on external interventions for induction. One common method is to injure the RPE/Bruch's membrane complex by either laser or mechanical intrusion. Laser-induced CNV in rodents is currently the standard animal model for most treatment evaluation experiments [18]. High-powered focused laser energy is used to break Bruch's membrane, causing acute injury and subsequent inflammation. The CNV is produced in a matter of hours and days rather than by the long-standing senescent degeneration and chronic inflammation of a natural or genetically-based condition. Anatomic discrepancies between naturally occurring CNV and laser-induced instances exist. For instance, the neural retina, which is not typically affected in human AMD, can be damaged by laser energy. Such neuroretinal changes could alter the local environment surrounding experimental CNV [14]. Furthermore, there are fundamental pathophysiological differences in this acute thermal-induced VEGF-dependent injury model versus chronic aging [19]. Another external intervention, though less commonly reported, is the alteration of the RPE and surrounding environment with the application of exogenous compounds injected into the subretinal space. By this method, stimulators of angiogenesis can be delivered in close proximity to the choroidal vasculature. Mechanical disruption of the RPE during the injection, along with angiogenic signals induced by the injected agent, can initiate the growth of choroidal neovessels into the subretinal space [20]. The subretinal injection of Matrigel [21,22], lipid hydroperoxide [24], polyethylene glycol (PEG) [25], and subretinal VEGF gene therapy [26] all have been described as CNV inducers in animal models. For example, after a Matrigel subretinal injection, CNV is initiated by the subretinal deposition of the extracellular matrix facilitating CNV development [21]. However, small CNV lesions can also be induced by subretinal injection of PBS [11,18]. This suggests that subretinal injection trauma alone can sufficiently damage Bruch's membrane to cause CNV [18]. Compared with laser injury, the subretinal injection models seem to have less adverse effects, such as severe inflammation and direct neuroretina damage [24]. Although laser models are reasonably consistent and result in CNV in approximately 80% of lesions [18], subretinal injection models proved to be more efficient and highly reliable, reaching up to 96% of the animals in the subretinal VEGF gene therapy model [26].

Therefore, it becomes clear that there are no ideal mice models of CNV. In this sense, the recent model that utilizes subretinal PEG to create a CNV in mice has shown promising results as described by Lyzogubov et al. [25]. The use of mice as experimental models in ophthalmology is prevalent common due to low cost, disease progression on a relatively short time-period and ease of carrying out genetic manipulation, even though mice lack an anatomic macula [14]. In this model, PEG injection activates the complement cascade and induces a dose-dependent CNV. An experimental CNV mouse model that uses a single subretinal injection of PEG seems an economical, simple, and quickly developed model. However, information in the literature about this model is appreciably limited (PubMed; accessed July 2018), and before being considered as a suitable model for the screening of new therapies, it should be refined, further tested and validated in other laboratories. Therefore, the aim of this study was to evaluate and validate the reliability and reproducibility of a rodent CNV model using the subretinal injection of PEG, previously described by Lyzogubov et al. [25], as a required step before accepting this model as suitable for testing new CNV therapies. The scientific community must understand that it is fundamental to completely characterize and adequately validate an animal model before using it for the evaluation of new potential treatments. Only in this way can the results obtained from experimental animals be adequately extrapolated and transferred to human clinical practice.

METHODS

Animals: The use of animals in this study was approved by the Animal Research and Welfare Ethics Committee of the University of Valladolid (Valladolid, Spain) and was authorized by the Farming and Ranching Agency of Junta de Castilla y León (Regional Government, Spain) in agreement with European (Council Directive 2010/63/UE) and Spanish regulations (RD 53/2013). This study was in accordance with the recommendations of the Association for Research in Vision and Ophthalmology for the Use of Animals in Ophthalmic and Vision Research. Thirty-two (n=32) wild-type male C57BL/6 mice (specific pathogen-free [SPF] colony, 8±1 weeks old, 24±1.5 g; Jackson Laboratory, Bar Harbor, ME) were used. The animals were randomly divided into Control 1 (PBS-injection, n=5), Control 2 (PBS-injection, n=9), and Experimental (PEG-injection, n=18) groups. The Control 1 animals were immediately sacrificed after the injection while the Control 2 and Experimental groups were further split into 5, 14 and 21-day follow-up groups (Table 1). Thus, four control groups and three experimental groups were used. Each animal group was individually housed in Type II conventional cages inside a specific experimental area at the animal facilities of the University of Valladolid. Each

experimental area had restricted access to a single researcher and followed a complete sanitary emptying procedure that includes washing and disinfecting the room and materials in advance to house the animals. The animals were kept under 12 h:12 h light-dark conditions at 22 °C and Lignocel 3–4 S (JRS GmbH + Co KG, Rosenberg, Germany) was used as bedding material. The animals had varied enrichment material in their cages and had free access to food (V1534–000 ssniff® R/M-H; ssniff Spezialdiäten GmbH, Soest, Germany) and water during the study. The selection of the species, type, breed and sex of the animals used in this study has been based on a previous publication [25] that described the rodent CNV model by subretinal injection of PEG and in the absence of evidence of gender difference in AMD prevalence [25,27]. This study was designed to use the minimum number of animals per experimental group that allows an adequate biostatistical analysis of the results and their possible extrapolation to humans.

Surgical technique: The following medical and surgical protocols were selected according to the species, sex, age and weight of the animals, as well as the requirements of the study performed. All the procedures described were performed in an operating room inside the animal facilities of the University of Valladolid. The surgical procedure was performed on both eyes in the Control 1 group. For the Control 2 group (PBS injection) and the Experimental group (PEG injection), only the right eye was injected. To carry out the surgical procedure, the animals were anesthetized by an intraperitoneal injection of ketamine (80–100 mg/kg; Imalgene 1000, Merial, Lyon, France) and xylazine (5–10 mg/kg; Rompún 2%, Bayer HealthCare, Kiel, Germany). Pedal and auricular reflexes were used to monitor the level of anaesthesia. Analgesia was applied by subcutaneous injection of butorphanol (0.5–3 mg/kg; Torbugesic® Vet, Fort Dodge Animal Health, Fort Dodge, IA). The periorbital area was cleansed by a solution of povidone iodine (5% Betadine®; Meda Manufacturing, Bordeaux, France). Cyclopentolate 1% (Colircusí Ciclopléjico®; Alcon Cusí S.A., Barcelona, Spain), phenylephrine 2.5% (Colircusí Fenilefrina®; Alcon Cusí S.A.) and 0.4% oxybuprocaine/0.1% tetracaine (Colircusí Anestésico Doble®; Alcon Cusí S.A.) were administered topically as mydriatic agents and as a local anaesthetic, respectively. An electric heating blanket was used to prevent hypothermia during the surgical procedure.

A single subretinal injection was administered per eye as described by Matsumoto et al. [28]. In brief, surgical procedures were performed under a Leica M844 surgical microscope (Leica Microsystems, Wetzlar, Germany). The conjunctiva was dissected using Vannas scissors (John Weiss & Son Ltd., Milton Keynes, UK). To prevent an increase of intraocular pressure, a corneal paracentesis at 1 mm anterior to the limbus was performed with a 30-gauge needle (Becton Dickinson, Franklin Lakes, NJ). A XenoWorks™ analog microinjection system (Sutter Instrument, Novato, CA) equipped with a NanoFil Hamilton 10 µl syringe (World Precision Instruments, Sarasota, FL) and a 33-gauge blunt needle (World Precision Instruments) was used for injections. A drop of hydroxypropyl methylcellulose (Methocel® 2%; OmniVision, Puchheim, Germany) over the cornea was used to facilitate fundus visualization through the microscope. The sclera was punctured at the pars plana on the superior temporal quadrant to introduce the 33-gauge blunt needle. A tunnel through the sclera and the choroid was then created until the subretinal space, between the neural retina and the RPE, was reached. Advancement of the needle was carefully monitored under the surgical microscope. One milligram of PEG-8 (mean molecular weight of 400; Spectrum Chemicals & Laboratory Products, Gardena, CA) diluted in 2 µl of PBS (Gibco; Invitrogen, Paisley, UK) or 2 µl of PBS (control eyes, Gobco, Invitrogen), were gently and slowly microinjected (in 10 s) into the subretinal space. Fresh PEG-8 dilutions were prepared for each experiment. Successful administration into the subretinal space was confirmed by the appearance of a subretinal bleb in the ocular fundus. Postoperative antibiotic treatment was established with topical ciprofloxacin (Oftacilox®, Alcon S.A.) twice a day for three days after the subretinal injection. Physical examination of the animals (such as activity, interaction with cage mates, general appearance) was performed daily throughout the study.

Table 1. Treatment groups and follow-up times.

Injected material	Animals (n)	Follow-up (days)
Control 1: PBS	5	0
Control 2: PBS	3	5
	3	14
	3	21
Experimental: PEG	6	5
	6	14
	6	21

PEG: polyethylene glycol; PBS: phosphate-buffered saline

Histological and immunohistochemical evaluation: At the designated times, the mice were sacrificed by CO_2 overdose according to the species, sex, age and weight of the animals. Control 1 mice were killed immediately after the injection of the second eye without allowing recovery from the anaesthesia. Control 2 (PBS-injected) and Experimental mice (PEG-injected) were killed at 5, 14 or 21 days after subretinal injection. A 10–0 nylon suture (Alcon, Fort Worth, TX) was

placed at the central superior sclera to facilitate sample orientation during tissue processing. Enucleation was performed to remove the entire ocular globe. The eyeballs were punctured at the limbus with a needle and immediately submerged in fixative (4% paraformaldehyde in 0.1 M-phosphate buffer; pH 7.4) for 24 h at room temperature. After fixation, samples were processed in an automatic tissue processor (Leica ASP300; Leica Microsystems, Wetzlar, Germany). One paraffin block of each eye was made and vertical serial 4-µm thick sections through the optic disc were obtained in a rotatory microtome (Microm HM340E; Microm International GmbH, Walldorf, Germany) until the identification of the injection site. Sections at the site of injection and around that point were used for this study.

Ocular sections for haematoxylin and eosin (HE) or Fontana-Masson (FM) staining were de-waxed in xylene, rehydrated in a series of descending alcohols (100°, 96° and 80°), rinsed in deionized distilled water, and stained with HE (Merck KGaA, Darmstadt, Germany) or FM. Stained sections were dehydrated in a series of ascending alcohols (96° and 100°), cleared in xylene, mounted, and coverslipped. Ocular sections for immunohistochemistry were de-waxed in xylene, rehydrated as described above, and rinsed in PBS (Gibco, Invitrogen). For antigen retrieval, sections were incubated in 0.01% trypsin (Sigma-Aldrich, Steinheim, Germany) in PBS (Gibco, Invitrogen) for 15 min at 37 °C. Then, the sections were immunostained for the phenotype-specific markers cytokeratin 8/18 (CK8/18; 1:25, Abcam plc., Cambridge, UK), isolectin B4 from *Griffonia simplicifolia* (IB4; 1:50, Molecular Probes, Eugene, OR), VEGF (1:50, Bioss Antibodies, Woburn, MA), and von Willebrand factor (vWF; 1:50, Millipore, Billerica, MA). Antibodies were diluted in PBS (Gibco, Invitrogen) containing 0.5% Triton X-100 (Sigma-Aldrich), and the sections were incubated overnight at 4 °C. The next day, the sections were washed in PBS (Gibco, Invitrogen). Thereafter, the corresponding species-specific secondary antibody conjugated to Alexa Fluor 488 or 568 (green or red, respectively; Thermo Fisher Scientific, Rockford, IL) was applied at a 1:200 dilution for 1 h. Nuclei were stained with 10 µg/ml 4',6-diamino-2-phenylindole dihydrochloride (blue; DAPI, Molecular Probes). Finally, sections were washed in PBS (Gibco, Invitrogen), mounted in an aqueous-based fluorescent mounting medium (Fluoromount-G; SouthernBiotech, Birmingham, AL) and coverslipped.

Control samples, in which the primary antibody was omitted, were processed in parallel, and no immunoreactivity was found in any case. The specificity of antibodies and IB4 had been previously tested [35,36] in our laboratory. Samples from a human eyelid cavernous haemangioma (courtesy of the IOBA Ocular Pathology Lab, University of Valladolid, Spain) were used as positive controls for the VEGF and vWF antibodies. Samples were analysed with a Leica DM4000B light microscope (Leica Microsystems) equipped for epifluorescence, and images were acquired with a Leica DFC490 (Leica Microsystems). Comparative studies of immunoreactivity expression were performed on images acquired at the same levels of exposure, intensity and gain. Brightness and contrast were minimally adjusted, and the final figures were composed with Pixelmator 3.4 Twist (Apple, Cupertino, CA).

Immunoreactivity semi-quantification was measured in ocular sections as previously described [29]. Two-channel micrographs were analysed using ImageJ software v. 1.49 (ImageJ; National Institutes of Health, Bethesda, MD). The micrographs were then split into different channels and each channel thresholded. To subtract background in the green channel (corresponding to the protein of interest), negative controls were used to set the threshold value, and the same value was used in all micrographs being analysed from the same experiment at the same time. The threshold for the blue channel, corresponding to the area of nuclei, was set according to the area stained. The mean gray value was measured by redirecting the measurement to the corresponding channel. The results, in arbitrary units, were the ratio of the mean gray value for the green channel to that obtained from the blue channel.

Statistical analysis: All data were collected in a database created in Excel (Microsoft Office Excel 2013, Microsoft Corporation, Redmond, WA) and subsequently analysed by the Student *t* test for independent samples. Each group of animals previously defined was studied as an independent unit of analysis. In all cases, a p value of less than 0.05 was considered statistically significant. Data were expressed as means ± standard deviations. Normality and homogeneity of variance assumptions were checked by the Shapiro-Wilk test and the robust Brown-Forsythe Levene-type test, respectively.

RESULTS

Surgical technique: Ocular evaluation under a surgical microscope ruled out the presence of ocular alteration before performing the surgical procedure. No adverse effects were detected beyond those induced by the subretinal injection procedure; thus, the previously described protocol was not modified. The subretinal injections were adequately performed in all three animal groups and resulted in localized retinal detachment, confirmed under surgical microscopy by the presence of subretinal blebs (Figure 1A, arrows). Eyes from the Control 1 group were evaluated immediately after the procedure (0 days) to confirm localized subretinal

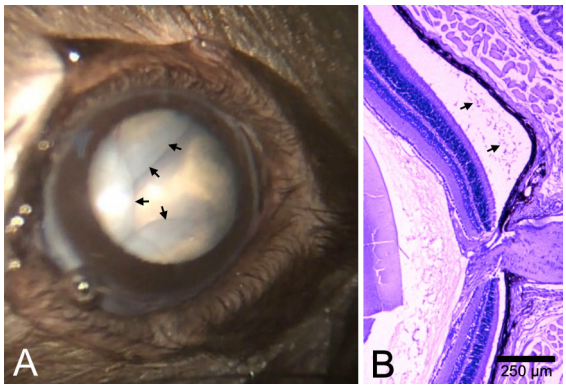

Figure 1. Ophthalmic and histological appearance immediately after subretinal injections of PBS. **A**: Subretinal blebs visualized by surgical microscopy immediately after subretinal injection (arrows, delimitation of retinal detachment extensions). **B**: Separation between the neuroretina and retinal pigment epithelium in the superior temporal quadrant of the eye (subretinal injection area). No significant damage was evident in the neuroretina or in the retinal pigment epithelium/choroid. Photoreceptor outer segment debris was present in the subretinal space (arrows). Haematoxylin and eosin staining, scale bar: 250 µm.

injections. Superior retinal detachments were histologically evident (Figure 1B). Photoreceptor outer segment debris was present between the separated neuroretina and RPE (Figure 1B, arrows). No other damage attributable to the injection procedure was observed in the neuroretina or in the RPE/choroid.

Histological evaluation: At 5 days of follow up, 2/3 PBS-injected eyes had retinal degeneration, disruption of the RPE and migration of pigmented cells (Figure 2A). In 1/3 mice, there was RPE vacuolization. In 4/6 PEG-injected eyes, there was a loss of normal retinal architecture and degeneration of the photoreceptor outer and inner segments (Figure 2B). Enlargement and vacuolization of the RPE cells, similar to that seen in the PBS-injected control eye, and the presence of pigmented clumps in the subretinal space were also evident. At 14 days of follow up, all of the PBS-injected eyes had subtle subretinal vacuolization and pigment cell migration with only a slight disruption of the photoreceptor outer segments (Figure 2C). 2/6 PEG-injected eyes had retinal degeneration and RPE/choroid modifications (Figure 2D). Pigment clumps and cell vacuolization in the RPE/choroid were also noted. At 21 days of follow up, none of the PBS-injected eyes presented either neuroretina or RPE/choroid degenerative modifications (Figure 2E). In some areas, 3/6 PEG-injected eyes had outer retinal degeneration and subtle RPE changes, such as RPE clumps and the migration of pigmented cells (Figure 2F).

To determine the composition of the subretinal pigmented clumps, ocular sections were stained with FM, which specifically identifies melanin granules that reduce silver nitrate to metallic silver. This specific staining revealed, in both PBS and PEG-injected eyes, the presence of melanin in the subretinal pigmented clumps at different time points (Figure 3A, arrowheads), as well as in the RPE layer and in the choroid (Figure 3A, arrows).

Immunohistochemical evaluation: To determine the origin of the subretinal pigmented cells, ocular sections were immunostained for CK8/18, the epithelial-type cytokeratins that are the major intermediate filaments in the RPE. Non-injected and PEG-injected eyes had positive immunoreactivity to CK8/18 in the RPE monolayer (Figure 3B and C, arrows). Positive cellular elements at the subretinal space were also observed in PEG-injected eyes (Figure 3C, arrowheads).

To evaluate the choroidal vasculature, ocular sections were immunostained with *Griffonia simplicifolia* isolectin B4 (IB4), a ligand that specifically binds terminal α-galactosyl residues expressed by endothelial cells and other cell types. In both the PBS- and PEG-injected eyes, IB4 was present in endothelial cells of the choroid (Figure 4A, B, arrows). PBS-injected eyes had a clearly recognizable network of small and medium arteries and arterioles, while in PEG-injected eyes, some vessel walls appeared diffusely thickened. IB4 immunoreactivity was significantly increased in PEG-injected eyes in comparison with that of PBS-injected eyes at all time points (Figure 4C).

To evaluate neovascularization, ocular sections were immunostained for VEGF, a soluble protein that stimulates vascular endothelial cell proliferation and is a potent inducer of angiogenesis. The sections were also stained for vWF, a glycoprotein that plays a major role in blood coagulation and is a widely used endothelial cell marker for studying angiogenesis/neovascularization. Both VEGF and vWF were present in the control sample from a human eyelid cavernous haemangioma, but neither was detectable in the retina/choroid area of the injected-eyes at any follow-up time (Figure 5).

DISCUSSION

While the treatment of CNV has improved in recent years, there is still little understanding of the cellular and molecular origins of the disease. Many of the improvements in clinical management have been based on information derived from the use of animal models that provide novel insights regarding CNV pathogenesis and possible new treatments. While some of these models have many of the clinical features of human CNV, the time course of development and progression and the anatomic features, such as lesion size and appearance, are dissimilar among the models. They also vary from the course

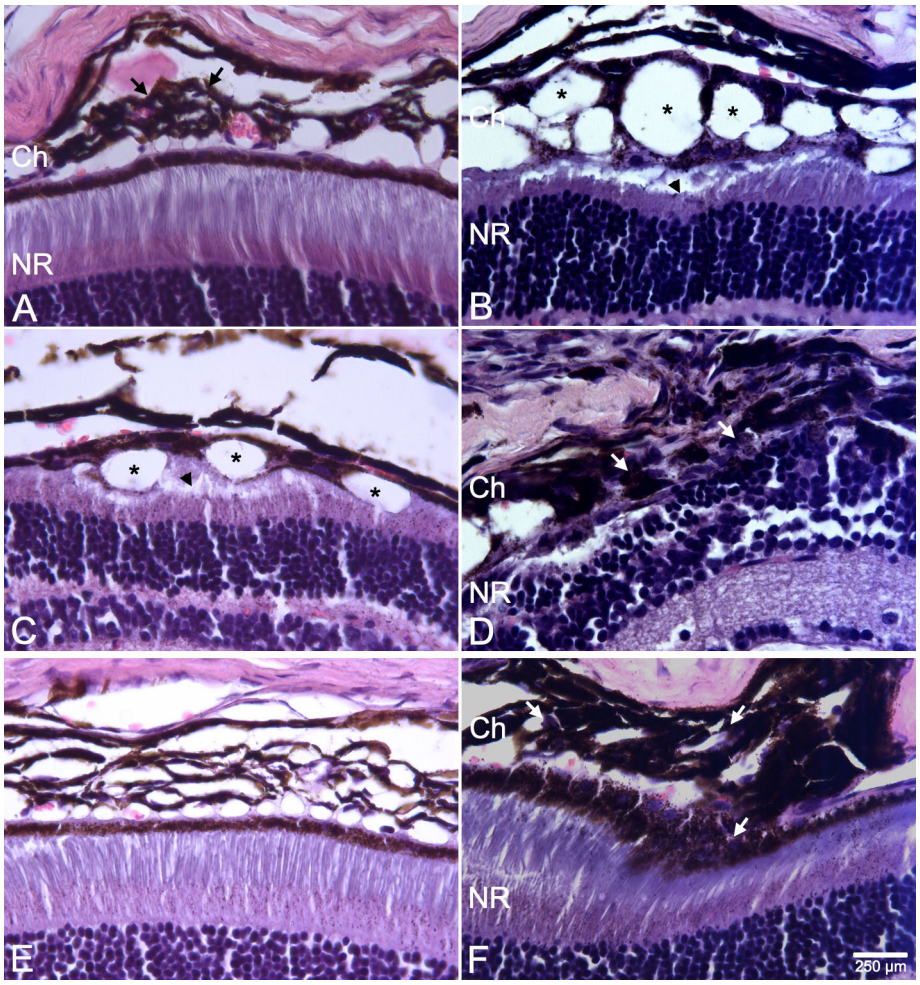

Figure 2. Haematoxylin and eosin (HE) stained retina-choroid sections from PBS- and PEG (1 mg)-injected eyes. Representative micrographs at 5 days after injection show (**A**) PBS-induced disruption of RPE/choroid cells (arrows) while (**B**) PEG-induced degeneration of photoreceptor outer segments (arrowhead), RPE cell enlargement, and vacuolization (asterisks). At 14 days, (**C**) PBS-injected eyes presented subretinal vacuolization (asterisks) and disruption of the photoreceptor outer segments (arrowhead), and (**D**) PEG-injected eyes revealed marked retinal degeneration and total RPE/choroid disruption (arrows). At 21 days, (**E**) PBS-injected eyes showed that the retina/choroid structures were preserved, while (**F**) PEG-injected eyes had RPE clumps and pigment cell migration (arrows). Ch: choroid; NR: neuroretina; PEG: polyethylene glycol. Scale bar: 25 µm.

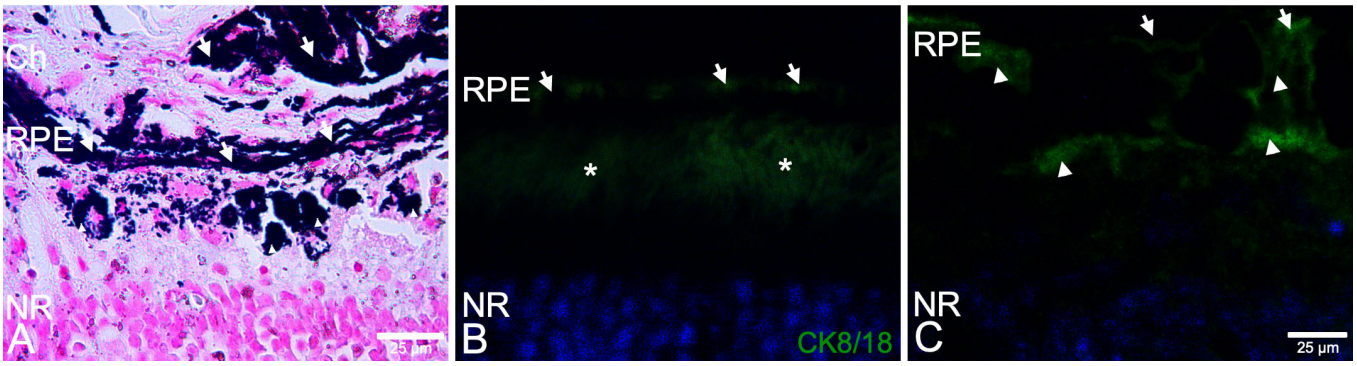

Figure 3. Fontana-Masson (FM) staining and cytokeratin 8/18 (CK8/18) immunofluorescence in retina-choroid sections from mice at 14 days after polyethylene glycol (PEG) injection. In these representative micrographs, (**A**) FM staining revealed the presence of melanin granules in the pigmented clumps at the subretinal space (arrowheads) and in the RPE and choroid (arrows). Black: melanin; pink-red: nuclei and cytoplasm. **B**: In non-injected mouse eyes, immunostaining of CK8/18 (green) was present in the monolayer of RPE cells (arrows). **C**: In PEG-injected eyes, CK8/18 was present in cellular elements at the subretinal space (arrowheads), as well as in the RPE cells (arrows). Asterisk: autofluorescence from photoreceptor outer segments; blue, DAPI-labelled nuclei. Ch: choroid; NR: neuroretina. Scale bar: 25 µm.

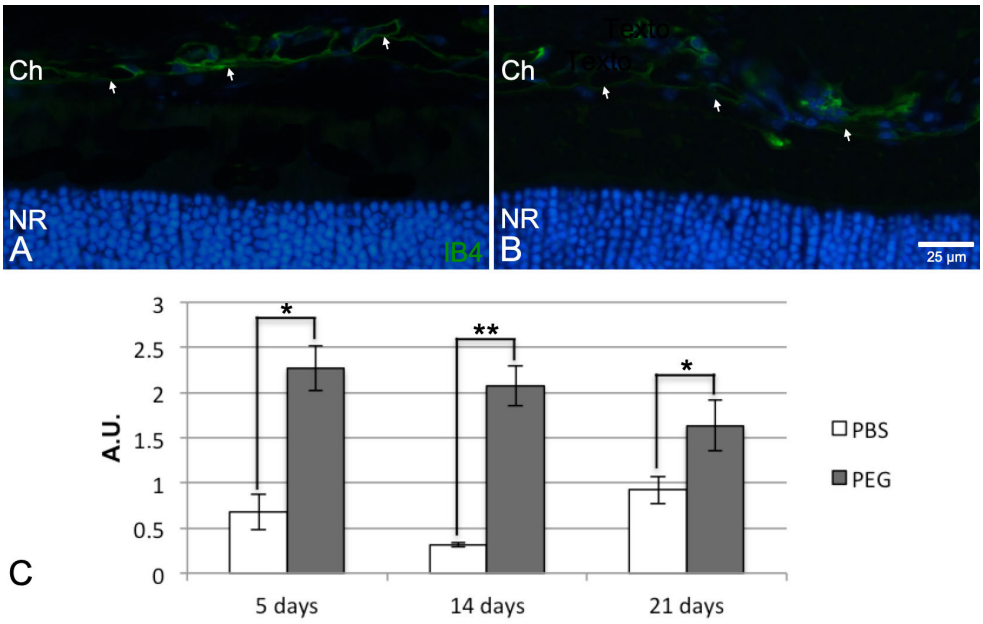

4. Isolectin B4 (IB4) immunofluorescence of retina/choroid sections from PBS- and PEG-injected eyes at 14 days after injection.IB4 immunostaining (green) revealed morphological differences in the choroidal vessel pattern between (**A**) PBS- and (**B**) PEG-injected eyes (arrows). Vessel walls of the PEG-injected eyes appeared diffusely thickened. Blue, DAPI-labelled nuclei; Ch, choroid; NR, neuroretina. Scale bar: 25 µm. **C**: Quantification of IB4 immunofluorescence in subretinal PBS- (white bars) and PEG-injected (black bars) mice. A.U.: arbitrary units. *p<0.05; **p<0.001 between subretinal PBS- and PEG-injected eyes at different time points. PEG: polyethylene glycol.

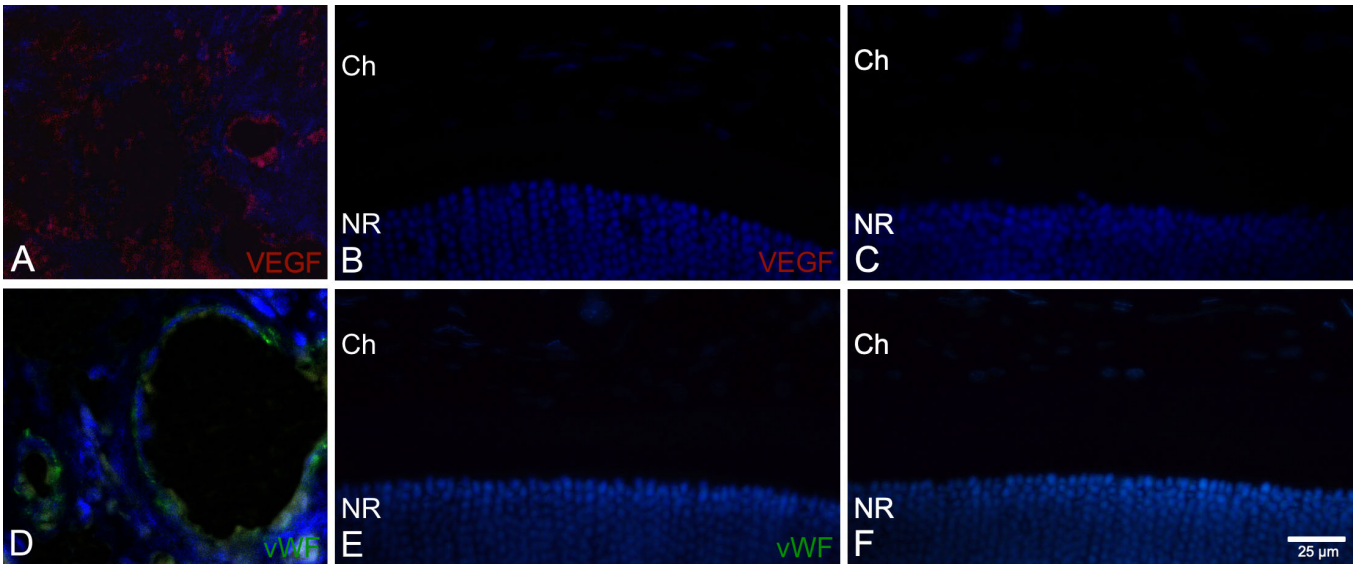

Figure 5. Vascular endothelial growth factor (VEFG) and von Willebrand factor (vWF) immunofluorescence in retina/choroid sections from PBS- and PEG-injected eyes at 14 days after injection. VEGF immunoreactivity (red) was evident in (**A**) a positive control sample from a human eyelid cavernous haemangioma, courtesy of the IOBA Ocular Pathology Lab, but was not apparent in the retina/choroid of the (**B**) PBS- or (**C**) PEG-injected eyes. Similarly, vWF immunoreactivity (green) was evident in (**D**) a positive control sample from a human eyelid cavernous haemangioma, but was not apparent in the retina/choroid of the (**E**) PBS- or (**F**) PEG-injected eyes. Blue, DAPI-labelled nuclei; Ch, choroid; NR, neuroretina; PEG: polyethylene glycol. Scale bar: 25 µm.

of the human disease [18]. Thus, the ideal animal model of human CNV has yet to be discovered.

In this scenario, Lyzogubov et al. [25] first described the subretinal injection of PEG to induce CNV in mice as an animal model of wet AMD. They have studied different PEG doses (0.125 to 2 mg) to induce CNV and evaluated the development of subretinal vessels at several time points (from 3 to 42 days). Furthermore, they examined the activation of the complement system after PEG injection that leads to CNV initiation, found a dose-dependent effect of PEG on the CNV size and observed a fully developed CNV and retinal degeneration at day 5 after injection. Finally, they concluded that the new model described stands out for being an inexpensive and accelerated mouse model of CNV with three distinct benefits: (1) the subretinal injection of PEG is technically easy to carry out; (2) there are rapid retina-choroid degenerative modifications after the procedure; and (3) the choroidal vessels show initial morphological changes.

In the present study, we evaluated the reliability and reproducibility of the promising mouse CNV model induced by subretinal injection of PEG described by Lyzogubov et al. [25]. We have focused our study on the histological investigation and immunohistochemical characterization of the retina-choroid degenerative modifications after the subretinal injection of PEG to induce CNV. We selected a dose of 1 mg of PEG based on the results of Lyzogubov et al. [25]. However, we found that the histopathological modifications were not homogeneously present among the PEG-injected eyes in our study. We did not observe new vessel growth at the time points studied, and the PBS-injected control eyes also showed retina/choroid morphological modifications similar to those observed in the PEG-injected eyes. The model described by Lyzogubov et al. [25] was based on the principles of intraocular complement activation. PEG activates the complement system that is critical in CNV induction and progression [30,31]. Furthermore, the angiogenic role of PEG has been described previously in myocardial ischemia [32]. However, our results revealed heterogeneous retina/choroid modifications among the animals without apparent neovascularization process.

The Control 1 group (time 0) in our study served to evaluate the potential direct damage to the retina/choroid due to the injection procedure, which was performed with extreme care. The use of both eyes, without recovery of the animals, was allowed to reduce the number of living animals in this experimental group, according to the 3Rs. Localized retinal detachment at the injection site, i.e., separation between retina and RPE, was induced by subretinal injection. However, we found no direct rupture of the neuroretina, RPE/choroid disorganization, or choroidal detachment with this technique. The Control 1 group also confirmed the reliability of the subretinal injection procedure, and thus, documented the suitability for delivering the test agents to the correct location within the eyes of the mice used in this study.

In the present study, PEG subretinal injection induced histological modifications including degeneration of the external retinal layer, marked disruption of the RPE/choroid with cellular vacuolization, and the presence of melanin-loaded RPE cells and pigmented clumps in the subretinal space. Our histological findings are consistent with those previously described by Lyzogubov et al. [25]. We also found that IB4 immunoreactivity, an endothelial cell marker, was significantly increased in the choroid of the PEG-injected eyes, and the choroidal vessel walls appeared diffusely thickened compared with PBS-injected animals. These findings are compatible with the onset of vascular alterations. Consistent with this, Lyzogubov et al. [25] reported increased expression of VEGF and the growth of endothelial cells penetrating Bruch's membrane after PEG treatment. However, we were unable to detect either VEGF or vWF immunoreactivity that might correspond to angiogenesis and neovascularization during our study. Interestingly, Lyzogubov et al. [33] later reported that a subretinal injection of a lower dose (0.5 mg) of PEG induced degenerative changes in RPE, but without consistent choroidal vessel growth. Furthermore, in our study, 5/9 animals from the PBS-injected control group showed tissue modifications in the retina/choroid region that were similar to those in the PEG-injected group. This finding suggests that the trauma of subretinal injection alone damages Bruch's membrane and may result in CNV, as previously described by Grossniklaus et al. [18].

In summary, our results indicate that the subretinal injection of PEG in mice induces retinal and choroidal degenerative modifications that mimic the initial steps of the CNV process. However, the ocular changes were heterogeneous among the animals and did not follow a consistent pattern over the 21 days of the study. Furthermore, the majority of the PBS-injected mice showed similar degenerative changes. We did not observe abnormal growth of new vessels originating from the choroidal vasculature, which is the main feature of human CNV [6]. On the contrary, the RPE modifications that we observed could be considered part of the pathologic features of dry AMD, as also observed by Lyzogubov et al. [33] using lower doses of PEG. In the present study, we only tested 1 mg of PEG and higher doses may be necessary to reproduce CNV in other laboratories, due to differences in the experimental conditions (such as subretinal injection style/location, mouse source, housing conditions). Furthermore,

our findings suggest that retina-choroid changes at early time points may be caused by the subretinal injection itself, which were reversible in PBS-injected, but not in PEG-injected, eyes. Future studies must clarify and confirm these points. However, due to the results described, we consider that this model does not consistently reproduce CNV, and other rodent models induced by subretinal injection of exogenous compounds, such as Matrigel, must be considered. It is desirable that animal models of CNV be efficient, reproducible, stable and sustainable over time. Such models should exhibit pathologic findings similar to those of human CNV, including growth patterns [34], while being inexpensive to produce and observable by in vivo imaging techniques. Considering that there are no ideal models of CNV as yet, we encourage the research community to continue characterizing and improving CNV models while exerting caution when choosing models that best suit experimental needs and prevent result misinterpretation.

ACKNOWLEDGMENTS

The authors acknowledge the assistance of Britt Bromberg, PhD (Xenofile Editing), for the final editing of this manuscript, and Antonio López-García, B.Sc. (IOBA, Spain), for technical assistance with immunostainings. This study was supported by EU Program FP7-PEOPLE-2013-IAPP (612218/3D-NET) and FEDER-CICYT (MAT2013–47501-CO2–1-R; Ministry of Economy and Competitiveness, Spain) Grants. I Fernandez- Bueno was supported by RETICS RD12/0034/0001, Instituto de Salud Carlos III, Spain. ML Alonso-Alonso was supported by Fondo Social Europeo (Operational Programme for Castille and Leon) and Consejería de Educación, Castille and Leon Regional Government Actions, Spain. This study was partially presented at The Association for Research in Vision and Ophthalmology (ARVO) 2016 Annual Meeting.

REFERENCES

1. Hasegawa E, Sweigard H, Husain D, Olivares AM, Chang B, Smith KE, Birsner AE, D'Amato RJ, Michaud NA, Han Y, Vavvas DG, Miller JW, Haider NB, Connor KM. Characterization of a spontaneous retinal neovascular mouse model. PLoS One 2014; 9:e106507-[PMID: 25188381].

2. Attebo K, Mitchell P, Smith W. Visual acuity and the causes of visual loss in Australia. The Blue Mountains Eye Study. Ophthalmology 1996; 103:357-64. [PMID: 8600410].

3. VanNewkirk MR, Nanjan MB, Wang JJ, Mitchell P, Taylor HR, McCarty CA. The prevalence of age-related maculopathy: the visual impairment project. Ophthalmology 2000; 107:1593-600. [PMID: 10919916].

4. Weih LM, VanNewkirk MR, McCarty CA, Taylor HR. Age-Specific Causes of Bilateral Visual Impairment. Arch Ophthalmol 2000; 118:264-9. [PMID: 10676793].

5. Friedman DS, O'Colmain BJ, Muñoz B, Tomany SC, McCarty C, de Jong PT, Nemesure B, Mitchell P, Kempen J. Eye Diseases Prevalence Research Group. Prevalence of Age-Related Macular Degeneration in the United States. Arch Ophthalmol 2004; 122:564-72. [PMID: 15078675].

6. Lim LS, Mitchell P, Seddon JM, Holz FG, Wong TY. Age-related macular degeneration. Lancet 2012; 379:1728-38. [PMID: 22559899].

7. Miller JW. Age-Related Macular Degeneration Revisited – Piecing the Puzzle: The LXIX Edward Jackson Memorial Lecture. Am J Ophthalmol 2013; 155:1-35.e13. [PMID: 23245386].

8. Klein R, Wang Q, Klein BE, Moss SE, Meuer SM. The relationship of age-related maculopathy, cataract, and glaucoma to visual acuity. Invest Ophthalmol Vis Sci 1995; 36:182-91. [PMID: 7822146].

9. Sarks SH. New vessel formation beneath the retinal pigment epithelium in senile eyes. Br J Ophthalmol 1973; 57:951-65. [PMID: 4788954].

10. Sarks SH. Ageing and degeneration in the macular region: a clinico-pathological study. Br J Ophthalmol 1976; 60:324-41. [PMID: 952802].

11. Sarks JP, Sarks SH, Killingsworth MC. Morphology of early choroidal neovascularisation in age-related macular degeneration: Correlation with activity. Eye (Lond) 1997; 11:515-22. [PMID: 9425418].

12. Green WR, Enger C. Age-related macular degeneration histopathologic studies. The 1992 Lorenz E. Zimmerman Lecture. Ophthalmology 1993; 100:1519-35. [PMID: 7692366].

13. Giani A, Thanos A, Roh MI, Connolly E, Trichonas G, Kim I, Gragoudas E, Vavvas D, Miller JW. In Vivo Evaluation of Laser-Induced Choroidal Neovascularization Using Spectral-Domain Optical Coherence Tomography. Investig Opthalmology Vis Sci. 2011; 52:3880–7.

14. Pennesi ME, Neuringer M, Courtney RJ. Animal models of age related macular degeneration. Mol Aspects Med 2012; 33:487-509. [PMID: 22705444].

15. Edwards AO, Malek G. Molecular genetics of AMD and current animal models. Angiogenesis 2007; 10:119-32. [PMID: 17372852].

16. Elizabeth Rakoczy P, Yu MJT, Nusinowitz S, Chang B, Heckenlively JR. Mouse models of age-related macular degeneration. Exp Eye Res 2006; 82:741-52. [PMID: 16325179].

17. Montezuma SR, Vavvas D, Miller JW. Review of the Ocular Angiogenesis Animal Models. Semin Ophthalmol 2009; 24:52-61. [PMID: 19373687].

18. Grossniklaus HE, Kang SJ, Berglin L. Animal models of choroidal and retinal neovascularization. Prog Retin Eye Res 2010; 29:500-19. [PMID: 20488255].

19. Chen J. Enhancing reliability of the laser-induced choroidal neovascularization mouse model: insights from a new study. Investig Opthalmology Vis Sci. 2014; 55:6535-[PMID: 25324347].

20. Oshima Y, Oshima S, Nambu H, Kachi S, Hackett SF, Melia M, Kaleko M, Connelly S, Esumi N, Zack DJ, Campochiaro PA. Increased expression of VEGF in retinal pigmented epithelial cells is not sufficient to cause choroidal neovascularization. J Cell Physiol 2004; 201:393-400. [PMID: 15389527].

21. Cao J, Zhao L, Li Y, Liu Y, Xiao W, Song Y, Luo L, Huang D, Yancopoulos GD, Wiegand SJ, Wen R. A Subretinal Matrigel Rat Choroidal Neovascularization (CNV) Model and Inhibition of CNV and Associated Inflammation and Fibrosis by VEGF Trap. Investig Opthalmology Vis Sci. 2010; 51:6009-17. [PMID: 20538989].

22. Qiu G, Stewart JM, Sadda S, Freda R, Lee S, Guven D, de Juan E Jr, Varner SE. A new model of experimental subretinal neovascularization in the rabbit. Exp Eye Res 2006; 83:141-52. [PMID: 16579984].

23. Oh H, Takagi H, Takagi C, Suzuma K, Otani A, Ishida K, Matsumura M, Ogura Y, Honda Y. The potential angiogenic role of macrophages in the formation of choroidal neovascular membranes. Invest Ophthalmol Vis Sci 1999; 40:1891-8. [PMID: 10440240].

24. Baba T, Bhutto IA, Merges C, Grebe R, Emmert D, McLeod DS, Armstrong D, Lutty GA. A rat model for choroidal neovascularization using subretinal lipid hydroperoxide injection. Am J Pathol 2010; 176:3085-97. [PMID: 20395434].

25. Lyzogubov VV, Tytarenko RG, Liu J, Bora NS, Bora PS. Polyethylene glycol (PEG)-induced mouse model of choroidal neovascularization. J Biol Chem 2011; 286:16229-37. [PMID: 21454496].

26. Schmack I, Berglin L, Nie X, Wen J, Kang SJ, Marcus AI, Yang H, Lynn MJ, Kapp JA, Grossniklaus HE. Modulation of choroidal neovascularization by subretinal injection of retinal pigment epithelium and polystyrene microbeads. Mol Vis 2009; 15:146-61. [PMID: 19158960].

27. Wong WL, Su X, Li X, Cheung CM, Klein R, Cheng CY, Wong TY. Global prevalence of age-related macular degeneration and disease burden projection for 2020 and 2040: a systematic review and meta-analysis. Lancet Glob Health 2014; 2:e106-16. [PMID: 25104651].

28. Matsumoto H, Miller JW, Vavvas DG. Retinal detachment model in rodents by subretinal injection of sodium hyaluronate. J Vis Exp 2013; 79:79-[PMID: 24056325].

29. Soriano-Romaní L, Contreras-Ruiz L, García-Posadas L, López-García A, Masli S, Diebold Y. Inflammatory Cytokine-Mediated Regulation of Thrombospondin-1 and CD36 in Conjunctival Cells. J Ocul Pharmacol Ther 2015; 31:419-28. [PMID: 26154920].

30. Moein Moghimi S, Hamad I, Bünger R, Andresen TL, Jørgensen K, Hunter AC, Baranji L, Rosivall L, Szebeni J. Activation of the Human Complement System by Cholesterol-Rich and PEGylated Liposomes—Modulation of Cholesterol-Rich Liposome-Mediated Complement Activation by Elevated Serum LDL and HDL Levels. J Liposome Res 2006; 16:167-74. [PMID: 16952871].

31. Hamad I, Hunter AC, Szebeni J, Moghimi SM. Poly(ethylene glycol)s generate complement activation products in human serum through increased alternative pathway turnover and a MASP-2-dependent process. Mol Immunol 2008; 46:225-32. [PMID: 18849076].

32. Pawliuk R, Leboulch P. POLYETHYLENE GLYCOL (PEG) POLYMERS FOR THE PROMOTION OF ANGIOGENESIS. 2001. p. Patent application WO 2001087312 A1.

33. Lyzogubov VV, Bora NS, Tytarenko RG, Bora PS. Polyethylene glycol induced mouse model of retinal degeneration. Exp Eye Res 2014; 127:143-52. [PMID: 25088354].

34. Grossniklaus HE, Green WR. Choroidal neovascularization. Am J Ophthalmol 2004; 137:496-503. [PMID: 15013874].

35. Fernandez-Bueno I, Jones R, Soriano-Romaní L, López-García A, Galvin O, Cheetham S, Diebold D. Characterization of retina neuroglia cellular and molecular modifications in diabetic Zucker Diabetic Fatty rats. IOVS 2017; 58:4925-33. .

36. Rodriguez-Crespo D, Di Lauro S, Singh A, Garcia-Gutierrez MT, Garrosa García M, Pastor JC, Fernandez-Bueno I, Srivastava GK. Triple-layered mixed co-culture model of RPE cells with neuroretina for evaluating the neuroprotective effects of adipose-MSCs. Cell Tissue Res 2014; 358:705-16. .

Articles are provided courtesy of Emory University and the Zhongshan Ophthalmic Center, Sun Yat-sen University, P.R. China. The print version of this article was created on 18 March 2019. This reflects all typographical corrections and errata to the article through that date. Details of any changes may be found in the online version of the article.